

TUTORIAL

QSP-IO: A Quantitative Systems Pharmacology Toolbox for Mechanistic Multiscale Modeling for Immuno-Oncology Applications

Richard J. Sové^{1,*} , Mohammad Jafarnejad¹, Chen Zhao¹, Hanwen Wang¹ , Huilin Ma¹ and Aleksander S. Popel^{1,2}

Immunotherapy has shown great potential in the treatment of cancer; however, only a fraction of patients respond to treatment, and many experience autoimmune-related side effects. The pharmaceutical industry has relied on mathematical models to study the behavior of candidate drugs and more recently, complex, whole-body, quantitative systems pharmacology (QSP) models have become increasingly popular for discovery and development. QSP modeling has the potential to discover novel predictive biomarkers as well as test the efficacy of treatment plans and combination therapies through virtual clinical trials. In this work, we present a QSP modeling platform for immuno-oncology (IO) that incorporates detailed mechanisms for important immune interactions. This modular platform allows for the construction of QSP models of IO with varying degrees of complexity based on the research questions. Finally, we demonstrate the use of the platform through two example applications of immune checkpoint therapy.

During the past decade, the development of immunotherapy has become one of the most exciting breakthroughs in cancer research. Extensive preclinical and clinical research efforts that investigated the relationship between immune response and tumor growth have demonstrated that our body's immune system, upon proper education and activation, does have the full potential to completely eradicate malignant tumors.^{1,2} Motivated by these discoveries, numerous therapeutics have been designed to modulate the activity of major immune cells toward enhanced recognition and killing of cancer cells through distinct mechanisms, the most successful being the immune checkpoint blockers, namely, antibodies against programmed cell death protein 1 (PD-1), programmed death ligand 1 (PD-L1) and cytotoxic T-lymphocyte-associated protein 4 (CTLA-4) pathways, which have now revolutionized the treatment standards for multiple cancer indications.^{3–5}

Besides these three commonly targeted checkpoints, numerous immune-targeting drugs have been widely investigated in clinical trials against cancers. Examples include drugs that target agents such as indoleamine 2,3-dioxygenase and interleukins⁶ or other immune cells (e.g., myeloid cells, dendritic cells).^{7,8} In addition, various treatment combinations of immunotherapies with other anticancer therapeutics (e.g., chemotherapy, antiangiogenic therapies, targeted tyrosine kinase inhibitors) have also been investigated.^{9–11} However, the large number of registered trials is by no means an indicator of clinical success (more than 3,000 immunotherapy trials in the United States alone, and more than 1,700 active trials testing PD-1/PD-L1 blockers with other anticancer therapies^{12,13}). In fact, the general response rates of immunotherapies (e.g., US Food and Drug Administration–approved PD-1/PD-L1 antibodies) in cancer patients are highly variable, and for many

cancer types only a small subset of patients would respond favorably even in biomarker-selected cohorts.^{10,14} Therefore, it is of significant translational value to develop an integrative mechanistic understanding of cancer biology, interpatient variability, and drug–target interactions using state-of-the-art, quantitative systems–level models to help answer critical questions throughout the immuno-oncology (IO) drug development life cycle (e.g., target selection, biomarker identification, trial optimization), with the ultimate goal to reduce clinical trial failures and improve treatment efficacies in patients.¹⁵

In the pharmaceutical industry, the concept of modeling and simulating biological processes has long been implemented to investigate the pharmacokinetic (PK) and pharmacodynamic (PD) properties of candidate drugs. In recent years, the emergence of complex mechanism-based, quantitative systems pharmacology (QSP) models has attracted increasing interest in translational research and has now become an essential component in the practice of model-informed drug discovery and development.^{16–21} Centered around the mechanisms of human physiology and pathogenesis, endogenous cellular dynamics and pharmacology, and disease-associated gene/protein signatures, which can all be translated quantitatively into patient-specific and disease-specific parameters to generate virtual patient cohorts and simulate trial results, these fit-for-purpose or platform-based QSP models have already proven to be useful throughout the drug development process in a wide range of therapeutic areas.^{18,22–25}

In the field of IO, a number of computational models that aligned closely with the concepts of QSP with varying degrees of physiological details about the immune system have been developed to characterize the complex cellular

¹Department of Biomedical Engineering, Johns Hopkins University School of Medicine, Baltimore, Maryland, USA; ²The Sidney Kimmel Comprehensive Cancer Center, Johns Hopkins University School of Medicine, Baltimore, Maryland, USA. *Correspondence: Richard J. Sové (rsove1@jhmi.edu)

Received: January 2, 2020; accepted: July 17, 2020. doi:10.1002/psp4.12546

dynamics that regulate the antitumor immune response elicited by pharmacological agents (many of the fit-for-purpose IO models are reviewed in ref. 15). Regarding the recent developments in platform-based IO models, Wang *et al.* constructed a detailed compartmentalized systems pharmacology model that considers both molecular-level (e.g., multiple ligand/receptor binding pairs) and cellular-level kinetics (e.g., the chain of events in immune-cancer interactions) to simulate personalized treatment outcomes in response to checkpoint inhibitors for patients with metastatic breast cancer.²⁶ Milberg *et al.*, based on the similar platform backbone, expanded the reaction dynamics of cell-cell interactions and reparameterized the new model using clinical trial data in melanoma; the authors then used their model to assess different treatment regimens of checkpoint inhibitors for simulated melanoma patient cohorts.²⁷ Jafarnejad *et al.* further enriched the platform with a mechanistic module of antigen processing and presentation; the extended model was then parameterized to investigate potential biomarkers of tumor regression and predict patient-specific response to neo-adjuvant anti-PD-1 therapy in non-small cell lung cancer using clinical data.²⁸ This platform has also been used to model combination therapies in triple negative breast cancer²⁹ and colorectal cancer.³⁰ These QSP modeling studies from our group suggested the potential translational values and efficiency of platform-based model formulation in the *in silico* investigation of complex human diseases, especially in IO where new mechanisms are being discovered and novel treatment modalities are being tested at a very rapid pace.

In this tutorial, we present QSP-IO, a modularized QSP modeling platform based in MATLAB (MathWorks, Natick, MA) that allows efficient formulation of physiology-based IO models and quantitative simulation of patient outcomes in response to different immunotherapy combinations. The equations implemented in QSP-IO are based on those implemented in Jafarnejad *et al.* with minor improvements outlined in the Modules section. This tutorial assumes the reader is able to run and edit scripts in MATLAB and has a basic understanding of the SimBiology toolbox. This tutorial does not require any specialized knowledge of QSP, although the interested reader is referred to the following articles: refs. 22,31,32

We first give an outline the platform, detailing the overall structure and workflow of modeling with QSP-IO, followed by a description of the biological rationale and mathematical representation of the different mechanistic modules within the integrative QSP-IO model platform. Then, through two examples that characterize the complex interplay between immune cells, cancer cells, checkpoints, antigen presentation, and targeted immunotherapy, we demonstrate how to construct mechanistic IO models from scratch by selecting and connecting modules in QSP-IO, and how such models, based on physiological and clinical constraints, are mathematically initialized and simulated to predict patient response. Finally, we discuss how QSP-IO as a modeling platform can be further enriched to provide insights into rising issues in IO from the computational perspective.

SOFTWARE PACKAGE OVERVIEW

This work presents a modular toolbox for assembling IO-based QSP models in MATLAB using SimBiology (MATLAB 2018b, MathWorks). The code can be downloaded from our GitHub page (www.github.com/popellab/qspro). Overall, our QSP platform is a modular, multicompartmental dynamical systems model of IO that aims to predict various biological features important to antitumor immune physiology; similar models were implemented in our recent work.²⁶⁻²⁸ QSP-IO allows the user to create a SimBiology model object in a MATLAB script by calling functions from our platform. This section describes the directory structure (Directory Structure section), the parameter structures (Parameter Structure and Input section), our initial conditions procedure (Initial Conditions section), and the overall workflow (Workflow section).

Directory structure

The repository is organized into the following five main directories: *@struct*, *model*, *parameters*, *scripts*, and *utils*. The *model* directory contains all the functions necessary to create and manipulate the SimBiology model object. The *parameters* directory contains the parameter files (see the Parameter Structure and Input section for more details), and the *scripts* directory contains the user-defined scripts for creating models. The *utils* directory contains useful functions for accessing and manipulating components of the model, and the *@struct* directory contains overloaded MATLAB functions (*mpower*, *mrdivide*, *mtimes*, *plus*, and *simplify*) to manipulate the parameter structure (see the Parameter Structure and Input section); note that the *@struct* directory must be added to the MATLAB path.

Parameter structure and input

Model parameters are stored as MATLAB structures that have the following three attributes: Value, Units, and Notes. Value and Units store the parameter's value and units, respectively, and the Notes attribute stores comments about that parameter that will get incorporated into the SimBiology object.

The model parameters are inputted into the model using a JavaScript Object Notation (JSON) file that can be edited with any plain text editor. All parameters have the fields of name, value, units, description, and source. The name field refers to the name of the parameter used by QSP-IO; a complete list of the parameter names required by each module is included in the supplemental material. The value, units, and description fields correspond to the Value, Units, and Notes properties of the model parameter structures in MATLAB, respectively. The source field is used to indicate the reference where the parameter value was found. If the model parameter is determined by other parameters, the source field can be set to "derived"; these parameters must have the fields *derived_from* and *expression*. The *derived_from* field is an array of strings naming the parameters on which it is dependent. The *expression* field is a string giving the relationship between the named parameters in the *derived_from* property. An example for two different parameters is given next. Notice that in the *expression* field on line 15, *p(1)* and *p(2)* correspond to the first and second entries of the *derived_from* array, respectively; the

parameters number of lymph nodes and diameter of lymph node must also be defined in the same file.

Listing 1: Sample JSON parameter file entries

```
{
  "name": "V_C",
  "value": 5,
  "units": "liter",
  "description": "Central compartment volume",
  "source": "doi: 10.1002/
    psp4 .12040"
},
{
  "name": "V_LN",
  "value": null,
  "units": "liter",

  "description": "Lymph Node compartment volume",
  "source": "derived",
  "derived_from": ["number of lymph nodes",
    "diameter of lymph node"],
  "expression": "p (1) *4/3* pi *(p (2)/2)^3"
},
```

Initial conditions

One challenge when facing large systems of ordinary differential equations is coming up with a set of realistic initial conditions to represent the state of the system at the beginning of the simulation. It is standard practice to treat the initial conditions as unknown parameters; however, in large systems, this introduces a large number of parameters. Milberg *et al.* overcame this issue by initializing the tumor to the desired size and set all other state variables to zero.²⁷ Although this solution overcomes the difficulty of having many unknown parameters, it results in a large tumor growth rate initially attributed to the delay in immune activation. Jafarnejad *et al.* overcame the latter difficulty by fixing the tumor to the desired size, then let the other state variables evolve until they reach steady state, then initialized the system with those values.²⁸ One concern with existing methods is that they could result in a potentially unrealistic behavior, for example, a realization where the tumor decreases in size artificially in the absence of therapy.

In our platform, the number of cancer cells is initialized to one cell, all other state variables are initialized to zero, and the simulation is run for a long period of time. The initial conditions are taken at the time where the volume reaches the target volume (specified by the user as a diameter; the target volume is calculated by assuming a spherical tumor). This procedure is meant to mimic cancer biology, where a normal cell mutates and becomes cancerous. Furthermore, any parameterization that would not reach the user-specified initial size would not represent a realistic cancer patient, thus these subjects are eliminated from further simulations.

Workflow

Briefly, the platform incorporates the description of cancer cell growth with a death rate dependent on the number of T cells present in the tumor compartment. The platform has detailed mechanisms for immune activation by modeling the release of antigen from dying cancer cells; antigen uptake by antigen presenting cells; the presentation of antigen to naïve T cells; and the activation, proliferation, and transport of T cells between the four compartments. QSP-IO also implements PK and PD models for immune checkpoint inhibitors of PD-1 and PD-L1. A summary of the model interactions is shown in **Figure 1a**. A detailed description of each module is presented in the following section.

A summary of the workflow for using the toolbox is shown in **Figure 1b**. First, the workflow involves calling the initialization function that creates an empty SimBiology object with four compartments (called C, P, T, and LN, which stand for central, peripheral, tumor, and lymph node, respectively). The volumes of each compartment are constant, except for the tumor compartment whose volume is determined based on the number of cancer and T cells in the tumor compartment (see the Cancer Module section for more details). Second, the modules are called, which adds the relevant equations to the SimBiology object. After the model is created, the initial conditions routine is run, which creates the initial conditions for all the species in the model. Finally, the simulation can be run with the defined treatment scheme. The toolbox also includes routines for visualizing the results of the simulation. Overall, our toolbox consists of seven modules that can be called independently to control the complexity of the model to suit the specific research questions.

MODULES

The QSP-IO platform currently consists of the following seven modules that may be added independently to build a QSP model: A cancer module, an antigen presentation module, an antigen module, a T cell module, a regulatory T cell (Treg) module, a checkpoint module, and a pharmacokinetics module. Only the cancer module is required, and all other modules are optional and can be omitted to decrease the complexity of the model. Because of the modular nature of QSP-IO, additional modules can be created by following the structure of the existing modules; more details on extending the model are provided in the Conclusions.

In the current version, the cancer, T cell, and antigen modules can be called multiple times to simulate different clones of cancer, T cells, and antigen, respectively. Having multiple cancer cell clones may be used, for example, to model a heterogeneous tumor having populations of cells with different growth rates, different sensitivities to T cell killing, or having different neo-antigens. Defining multiple T cell clones may be used to model subpopulations of T cells that recognize different neo-antigens. Similarly, the antigen module can be called multiple times to simulate different antigens (including the effect of having competing self-peptides). In addition, the pharmacokinetics module can be called to simulate administration of multiple drugs. **Table 1** gives a summary of the modules

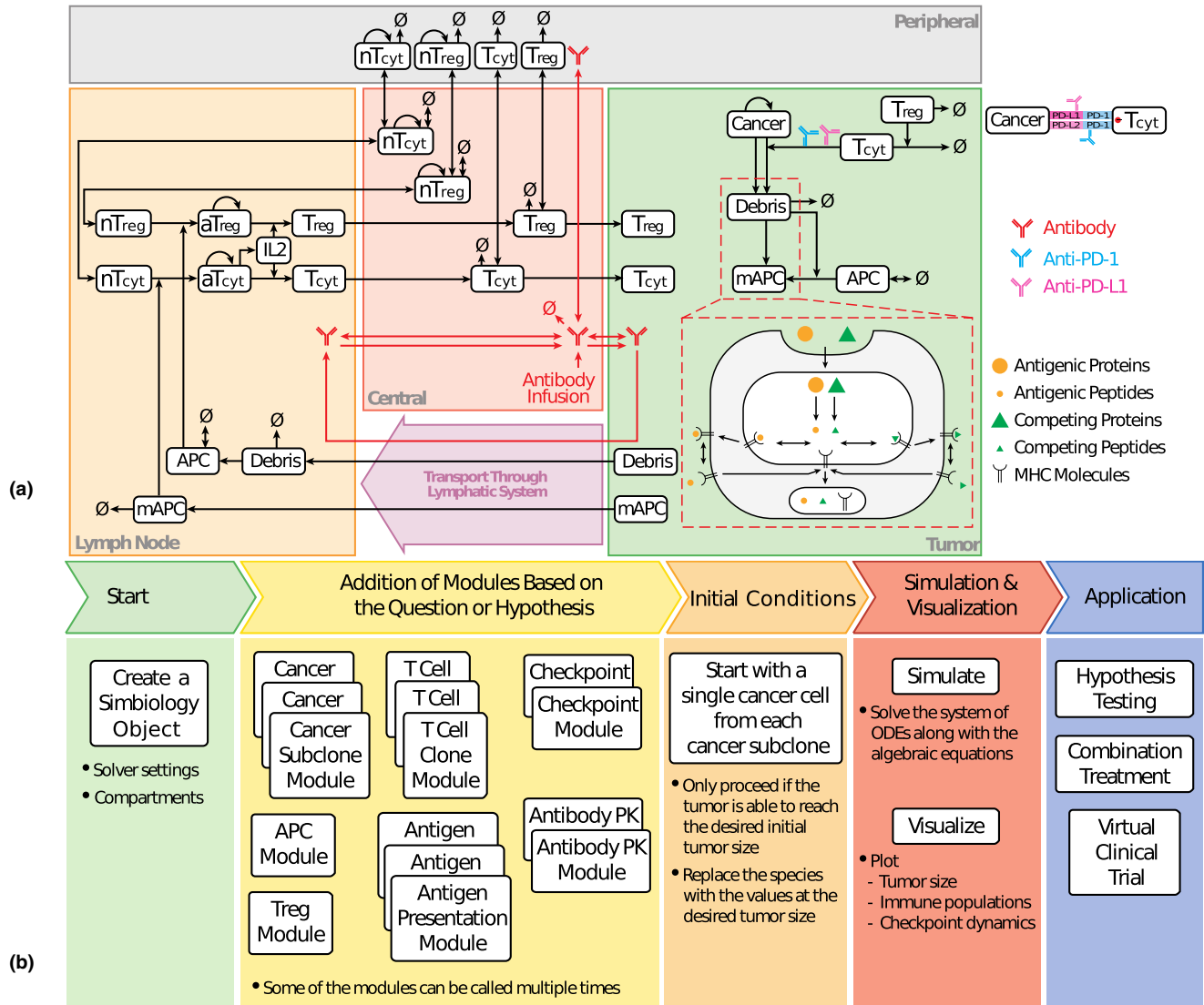


Figure 1 (a) Diagram of immuno-oncology quantitative systems pharmacology (QSP) model interactions. Naïve and mature antigen presenting cells are represented by APC and mAPC, respectively, naïve, proliferating and mature T cells are represented by nT, aT, T_{cyt} and regulatory T cells are represented by T_{reg}. (b) Workflow for creating a model in QSP-IO. The user starts by creating a SimBiology object using the QSP-IO’s initialization function. Module can be added to include the necessary detail in the model based on the research questions. The initial conditions are then generated based on the model parameters using the novel initial conditions procedure. Finally, the simulations can be run using standard SimBiology functions and visualization can be performed using MATLAB plot functions or using QSP-IO’s plotting function.

included in QSP-IO at the time of this writing; the modules are listed in the suggested order in which they should be called.

Cancer module

The number of cancer cells in the tumor, C , is given by the following:

$$\frac{dC}{dt} = k_{\text{growth}} C \left(1 - \frac{C}{C_{\text{max}}} \right) - \left(k_{\text{innate}} + k_{T_{\text{cell}}} \frac{T}{T+C} (1 - H_{\text{PD1}}) \right) C, \quad (1)$$

where the first term on the right represents the rate of cancer cell proliferation and the second term represents the rate of cancer cell death. Cancer cell proliferation is modeled by logistic growth as done in refs. 33 and 34 with maximal

growth rate, k_{growth} , and carrying capacity, C_{max} . Cancer cell death is assumed to be attributed to two mechanisms: death attributed to the innate immune system using first-order kinetics with rate constant, k_{innate} , and death attributed to cytotoxic T cells simulated by Michaelis-Menten kinetics with maximal death rate, $k_{T_{\text{cell}}}$, and the number of T cells in the tumor compartment, T . H_{PD1} is the fraction of T cell inhibition due to the PD-1 checkpoint, calculated according to:

$$H_{\text{PD1}} = \frac{X^n}{X^n + \text{PD1}_{50}^n}$$

where $X = \text{Asyn}[Y_1]$ (see the Immune Checkpoint Module section) is the number of PD1/PDL1 complexes

Table 1 Summary of modules

Module	Required	Number of calls	Dependencies
Cancer	Yes	Unlimited	None
T cell	No	Unlimited	Cancer
Treg	No	1	Cancer, T cell
Antigen presenting cell	No	1	Cancer
Antigen	No	Unlimited	Cancer, T cell
Immune checkpoint	No	1	Cancer, T cell

in the immune synapse between T cells and cancer cells, $PD1_{50}$ is the number of complexes for half-maximal T cell inhibition from the PD-1 checkpoint, and n is the Hill coefficient.

When modeling multiple cancer clones, Eq. 1 is used to calculate the number of cancer cells for each clone and the logistic growth term changes as follows:

$$k_{\text{growth}} C \left(1 - \frac{C}{C_{\text{max}}}\right) \rightarrow k_{\text{growth},i} C_i \left(1 - \frac{C_{\text{total}}}{C_{\text{max}}}\right),$$

where C_i is the i^{th} cancer clone and C_{total} is the total number of cancer cells. The maximal growth rate constant can be different for each cancer clone. Note that this assumes that all cancer clones are in competition for the same limiting resources.

Similarly, when modeling multiple T cell clones, the rate of cancer cell death from T cells becomes

$$k_{T_{\text{cell}}} \frac{T}{T+C} \rightarrow \sum_i k_{T_{\text{cell},i}} \frac{T_i}{T_{\text{total}} + C_{\text{total}}},$$

where T_i is the i^{th} T cell clone and T_{total} is the total number of T cells.

The tumor compartment volume, V_T , is then calculated based on the number of cancer cells and T cells in the tumor compartment according to:

$$V_T = V_{\text{cancer}} C_{\text{total}} + V_{T_{\text{cell}}} (T_{\text{total}} + T_{\text{reg}}) + V_{T_{\text{min}}}, \quad (2)$$

where V_{cancer} and $V_{T_{\text{cell}}}$ are the volumes of single cancer cells and T cells, respectively. $V_{T_{\text{min}}}$ is the minimum volume of the

tumor compartment, included to avoid a zero tumor compartment volume. Although this term has very little effect on the solution, it becomes more important at low tumor volumes; the tumor volume will tend toward $V_{T_{\text{min}}}$ as the number of cells in the tumor go to zero. Biologically, $V_{T_{\text{min}}}$ may be interpreted as the volume of the extracellular matrix or interstitial space around the tumor when the volume is small. The volume of other immune cells such as natural killer (NK) cells, tumor associated macrophages, and cancer-associated fibroblasts are not considered, but may be addressed in future work.

In Eq. 2, C_{total} and T_{total} include dead cancer and T cells, because the volume of the tumor would not change instantly following cell death. The dead cells are assumed to clear with first-order kinetics with rate constant k_{clear} . Including the T cells and dead cells in the volume calculation allows for the model to capture the pseudo-progression phenomenon observed in clinical settings³⁵ where the tumor appears to be growing while the number of viable cancer cells are decreasing (see **Figure 2**). In this simulation, the number of viable cancer cells reach a maximum in 50 days, whereas the tumor reaches its maximum volume at 294 days; this apparent discrepancy is attributed to the presence of T cells and dead cancer/T cells in the tumor. Once the number of viable cancer cells is low, the T cells deplete from the tumor. The tumor volume begins to decrease when number of cancer cells are low enough that the rate of death is less than the rate of dead cell clearance.

Antigen presenting cell module

The number of antigen presenting cells (APCs) are simulated in the tumor and the tumor-draining lymph node compartments. In our platform, we consider both naïve APCs and mature APCs. The APCs are assumed to mature in the tumor compartment where they are exposed to maturation cytokines, c . Mature APCs can migrate from the tumor to the lymph node,^{36–38} where they will present the antigen to activate naïve T cells.

The number of naïve APCs, D_i , are calculated in both compartments ($i = T, \text{LN}$) by assuming first-order kinetics about a target density, ρ_i^D , with rate constant, k_D , according to:

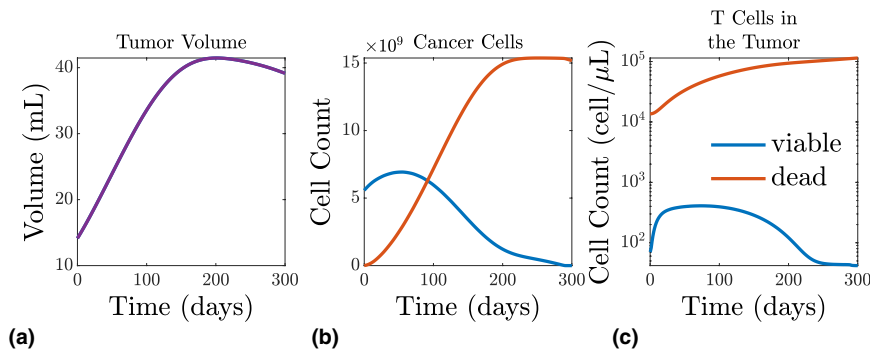


Figure 2 (a) Tumor volume as a function of time. (b) Number of viable (blue) and dead (red) cancer cells as a function of time. (c) Cell count for viable (blue) and exhausted (red) T cells as a function of time. The parameters from example 1 were used with cell clearance rate ($k_{\text{clear}} = 0.001 \text{ day}^{-1}$) and rate of cancer death from T cells ($k_{T_{\text{cell}}} = 8.7 \text{ day}^{-1}$) to demonstrate the pseudo-progression phenomenon.

$$\frac{dD_T}{dt} = k_D(\rho_T^D V_T - D_T) - k_{mat} \frac{[c]}{[c] + [c]_{50}} D_T \quad (3a)$$

$$\frac{dD_{LN}}{dt} = k_D(\rho_{LN}^D V_{LN} - D_{LN}), \quad (3b)$$

where the last term in Eq. 3a represents the rate of maturation; with maximal rate, k_{mat} , and Michaelis-Menten constant, $[c]_{50}$.^{39,40} The mature APCs, \hat{D}_i , are described by the following,

$$\frac{d\hat{D}_T}{dt} = k_{mat} \frac{[c]}{[c] + [c]_{50}} D_T - (k_{\hat{D}} + k_{mig}) \hat{D}_T \quad (4a)$$

$$\frac{d\hat{D}_{LN}}{dt} = k_{mig} \hat{D}_T - k_{\hat{D}} \hat{D}_{LN}, \quad (4b)$$

where k_{mig} is the first-order rate constant for the rate of migration to the lymph nodes from the tumor.

The maturation cytokines, c , are calculated according to:

$$\frac{d}{dt}(V_T[c]) = k_c([c]_0 - [c])V_T + k_{T_{cell}} \frac{TC}{T+C} (1 - H_{PD1})x_c, \quad (5)$$

where the first term on the right represents the first-order kinetics about $[c]_0$ with rate constant, k_c .³⁹ The second term represents the increased rate of cytokine release attributed to inflammation, measured by the rate of T cell killing given in Eq. 1 with the constant, x_c , representing the amount of cytokines released per cancer cell death because of T cells.

Antigen module

The antigen module models the release of antigen from lysed cancer cells, the uptake by mature APCs, degradation of antigen in the APC endosomes, and the presentation of antigen-major histocompatibility complex (MHC) on the surface of APCs.³⁹⁻⁴¹ The equation governing the antigen concentration, $[P]_T$, in the tumor is given by

$$\frac{d}{dt}(V_T[P]_T) = n_{clones}[P]_0 V_T \left(k_{death} + k_{T_{cell}} \frac{T}{T+C} (1 - H_{PD1}) \right) C - (k_{up} + k_{deg})[P]_T V_T, \quad (6)$$

where the first term on the right is the number of antigen clones represented, n_{clones} , times the concentration of a single antigen clone in a cancer cell, $[P]_0$, times the rate of cancer cell death. The second term on the right is the first-order uptake of antigen by APCs, with rate constant k_{up} and the first-order degradation in the extracellular space with rate constant, k_{deg} .

The equations governing the concentration of antigen, $[P]_e$, and epitope, $[p]_e$, in the endosomes of APCs are given by

$$\frac{d[P]_e}{dt} = k_{up}[P]_T - k_{deg}^P [P]_e \quad (7a)$$

$$V_e \frac{d[p]}{dt} = k_{deg}^P [P]_e V_e + k_{off}[Mp]_e A_e - (k_{on}[M]_e A_e + k_{deg}^p V_e) [p] \quad (7b)$$

where V_e and A_e are the volume and surface area of the endosomal compartment, respectively; k_{deg}^P and k_{deg}^p are the rate constants for antigen and epitope degradation, respectively; and k_{on} and k_{off} are the rate constants for antigen-MHC binding kinetics.

The following equations govern the binding of antigen epitope, p , to MHC, M , to form the antigen-MHC complex, Mp , in the endosomes (subscript e) and on the surface of APCs (subscript s).

$$A_e \frac{d[M]_e}{dt} = k_{off}[Mp]_e A_e + k_{in}[M]_s A_s - (k_{on}[p] + k_{out}) [M]_e A_e \quad (8a)$$

$$A_s \frac{d[M]_s}{dt} = k_{off}[Mp]_s A_s + k_{out}[M]_e A_e - k_{in}[M]_s A_s \quad (8b)$$

$$A_e \frac{d[Mp]_e}{dt} = k_{on}[p] [M]_e A_e + k_{in}[Mp]_s A_s - (k_{off} + k_{out}) [Mp]_e A_e \quad (8c)$$

$$A_e \frac{d[Mp]_s}{dt} = k_{out}[Mp]_e A_e - (k_{off} + k_{in}) [Mp]_s A_s, \quad (8d)$$

where A_e and A_s are the surface areas of the endosomes and APCs, respectively, and k_{in} and k_{out} are the rate constants for MHC internalization and externalization, respectively. Note that in Eqs. 7 and 8, the concentrations of M and Mp are per unit area.

T cell module

In the T cell module, we model the activation of naïve CD8+ T cells, the proliferation of activated T cells and transport of mature, activated, cytotoxic T cells. This module is also used by the Treg module to model the activation, proliferation, and transport of regulatory T cells (see the Regulatory T Cells section).

Naïve T cells. The number of naïve T cells are modeled in the central, peripheral, and tumor-draining lymph node compartments.^{42,43} In the central compartment, naïve T cells, \mathcal{N}_C , are modeled according to:

$$\frac{d\mathcal{N}_C}{dt} = \sigma + k_{prolif} \frac{\mathcal{N}_C}{K_m + \mathcal{N}_C} + \sum_{i=P, LN} (q_i^{out} \mathcal{N}_i - q_i^{in} \mathcal{N}_C) - k_{death}^{\mathcal{N}} \mathcal{N}_C, \quad (9)$$

where the first term on the right represents the rate of release of naïve T cells from the thymus described by zero-order kinetics with rate constant, σ , the second term represents the rate of proliferation modeled by Michaelis-Menten kinetics with maximum proliferation rate, k_{prolif} , and Michaelis constant, K_m . The third term on the right represents the transport between compartments using first-order kinetics with rate constants q_P^{in} , q_{LN}^{in} , q_P^{out} , and q_{LN}^{out} representing the rates for entry and exit of the peripheral and lymph node compartments. The last term on the right is the first-order death term.

Similarly, naïve T cells in the peripheral and tumor-draining lymph node compartments are given by the following:

$$\frac{d\mathcal{N}_P}{dt} = k_{prolif} \frac{\mathcal{N}_P}{K_m + \mathcal{N}_P} + q_P^{in} \mathcal{N}_C - q_P^{out} \mathcal{N}_P - k_{death}^{\mathcal{N}} \mathcal{N}_P \quad (10a)$$

$$\frac{dN_{LN}}{dt} = q_{LN}^{in} N_C - q_{LN}^{out} N_{LN} - k_{act} \frac{n_{sites} \hat{D}_T}{n_{sites} \hat{D}_T + T_{total}} \frac{[Mp]_s}{[Mp]_s + K_{m,p}} H_p N_{LN} \quad (10b)$$

where n_{sites} is the maximum number of T cell binding sites on the APCs. The rate of activation is assumed to be dependent on the number of APCs in the tumor and the number of antigen-MHC molecules presented on the surface of APCs. H_p is the fraction of activation due to T cell receptor (TCR) binding; see the T Cell Activation section for details.

T cell activation. The activation of naïve T cells by mature APCs is modeled by considering the interaction between TCRs on naïve T cells and antigen-MHC complexes on mature APCs. This engagement is modeled based on kinetic proofreading with limited signaling that was shown by Lever *et al.*⁴⁴ to best represent our understanding of T cell activation. Kinetic proofreading with limited signaling captures the presence of an optimum in T cell activation with respect to binding affinity of the TCR with antigen-MHC complex, which is observed at all levels of antigen-MHC.⁴⁴ The activation of the TCR is modeled by:

$$C_{tot} = \frac{1}{2} \left(Mp_s + TCR_{tot} + K_D - \sqrt{(Mp_s + TCR_{tot} + K_D)^2 - 4Mp_s TCR_{tot}} \right) \quad (11a)$$

$$TCR_{active} = \left(\frac{k_{off}^{TCR}}{k_{off}^{TCR} + \phi} \right) \left(\frac{k_p}{k_p + k_{off}^{TCR}} \right)^m C_{tot}, \quad (11b)$$

where Mp_s is the total amount of antigen-MHC complex on the surface of mature APCs, TCR_{tot} is the total amount of TCR on naïve T cells, K_D is the binding affinity ($k_{on}^{TCR}/k_{off}^{TCR}$) of TCR binding to antigen-MHC complex, C_{tot} is the total TCR-antigen-MHC complex, k_p is the modification rate, ϕ is the modification rate to the nonsignaling state, and m is the number of intermediate states. TCR_{active} was then related to the activation rate of naïve T cells by mature APCs using the following Hill function,

$$H_p = \frac{TCR_{active}}{TCR_{active} + K_{p,50}}, \quad (12)$$

where $K_{p,50}$ is the half-maximal level for T cell activation.

T cell proliferation. The number of first generation of proliferating T cells, \mathcal{P} , are calculated according to:

$$\frac{d\mathcal{P}}{dt} = n_{clones} k_{act} \frac{n_{sites} \hat{D}_{LN}}{n_{sites} \hat{D}_{LN} + T_{total}} \frac{[Mp]_s}{[Mp]_s + K_{m,p}} H_p N_{LN} - k_{pro} \mathcal{P}, \quad (13)$$

where the first term represents the rate of activation and the second term represents the rate of proliferation.

Assuming the T cells have a division destiny of N and that proliferation is in quasi-steady state, the number of proliferating T cells in the N^{th} generation is given by $2^N \mathcal{P}$. Recent work suggests that the division destiny is dependent on TCR binding, costimulatory signals, and the presence of interleukin-2 (IL2) and that each of these contributions are additive⁴⁵ such that,

$$N = N_{TCR} + N_{costim} + N_{IL2} \quad (14a)$$

$$N_{IL2} = \Delta N \frac{[IL2]}{[IL2] + [IL2]_{50}} \quad (14b)$$

In the present work, N_{TCR} and N_{costim} are assumed to be constant; however, future work will include variable N_{TCR} dependent on H_p from the kinetic proofreading model described in the T Cell Activation section.

IL2 is assumed to be secreted from proliferating T cells and is consumed by both proliferating regulatory T cells and proliferating cytotoxic T cells. The equation governing IL2 concentration is given by,

$$V_{LN} \frac{d[IL2]}{dt} = k_{sec} \mathcal{P}_{total} - k_{deg}^{IL2} [IL2] V_{LN} - k_{cons} \left(T_{LN} + T_{LN}^{Treg} \frac{[IL2]}{[IL2]_{50} + [IL2]} + T_{LN}^{Treg} \frac{[IL2]}{[IL2]_{50}^{Treg} + [IL2]} \right), \quad (15)$$

where T_{LN} and T_{LN}^{Treg} are the number of cytotoxic and regulatory T cells in the lymph node compartment, respectively.

Activated T cell distribution. T cell transport between compartments is modeled by first-order dynamics in the same way as with naïve T cells.⁴⁶ The rate of transport between the central and tumor compartments was assumed to scale with tumor volume. The equations governing the number of mature, activated, cytotoxic T cells in the four compartments are given by,

$$\frac{dT_C}{dt} = q_P^{out} T_P + q_{LN}^{out} T_{LN} - (q_P^{in} + q_T^{in} V_T + k_{death}^T) T_C \quad (16a)$$

$$\frac{dT_P}{dt} = q_P^{in} T_C + q_P^{out} T_P - k_{death}^T T_P \quad (16b)$$

$$\frac{dT}{dt} = q_T^{in} V_T T_C \left(k_{death}^T + k_{Treg} \frac{T_{reg}}{C_{total} + T_{total}} + k_C \frac{C}{C_{total} + T_{total}} \right) T \quad (16c)$$

$$\frac{dT_{LN}}{dt} = 2^N k_{pro} \mathcal{P} - q_{LN}^{out} T_{LN} - k_{death}^T T_{LN}, \quad (16d)$$

where k_{Treg} is the rate constant for T cell exhaustion by Tregs, k_C is the rate constant for T cell exhaustion by cancer cells. As with the cancer module, the user may define multiple clones of cytotoxic T cells, in which case the equations will be introduced for each clone, and the new clones will be added to T_{total} .

Regulatory T cells. The Treg module models regulatory T cells in all four compartments using the same equations as the T cell module with minor differences. First, the induction of Tregs in the tumor-draining lymph nodes are modeled using Eqs. 10b and 13 with the difference that Tregs are induced by presentation of self-reactive peptides on immature APCs,⁴⁷ thus the activation term becomes:

$$k_{act} \frac{n_{sites} \hat{D}_{LN}}{n_{sites} \hat{D}_{LN} + T_{total}} \frac{[Mp]_s}{[Mp]_s + K_{m,p}} H_p \rightarrow k_{act} \frac{n_{sites} D_{LN}}{n_{sites} D_{LN} + T_{total}} \frac{[Mp]_s}{[Mp]_s + K_{m,p}} H_p.$$

Second, the exhaustion terms from Tregs and cancer cells in Eq. 16c become zero. In addition, both natural and induced Tregs are accounted for in this module, but are both pooled together as Tregs. Natural Tregs are directly derived in the thymus and enter the blood.⁴⁸ The dynamics of the natural Tregs are modeled using an additional zero-order term in the central compartment. Finally, the number of Tregs is added to the T cell killing of cancer cells term used in Eqs. 1, 5 and 6 as follows:

$$k_{T_{\text{cell}}} \frac{T}{T+C} \rightarrow k_{T_{\text{cell}}} \frac{T}{T+T_{\text{reg}}+C}.$$

Immune checkpoint module

Interactions between PD-1 on T cell with PD-L1 and PD-L2 on cancer cell are modeled within an additional compartment that represents the immunological synapse between the two cells.⁴⁹ Different antibodies against these immune checkpoint molecules can be modeled. In this example, we have represented the currently approved bivalent antibodies against PD-1 and PD-L1. The equations governing the PD-1/PD-L1/PD-L2 checkpoints and the antibodies targeting them are as follows:

$$\frac{d[YY_1]}{dt} = k_{\text{on}}^{YY_1} [Y][Y_1] - k_{\text{off}}^{YY_1} [YY_1] \quad (17a)$$

$$\frac{d[YY_2]}{dt} = k_{\text{on}}^{YY_2} [Y][Y_2] - k_{\text{off}}^{YY_2} [YY_2] \quad (17b)$$

$$\frac{d[YA]}{dt} = \frac{2}{\gamma_T} k_{\text{on}}^{YA} [Y][A] - k_{\text{off}}^{YA} [YA] \quad (17c)$$

$$\frac{d[YAY]}{dt} = \frac{\chi}{A_{\text{syn}} d_{\text{syn}} N_A} k_{\text{on}}^{YAY} [YA][Y] - 2k_{\text{off}}^{YAY} [YAY] \quad (17d)$$

$$\frac{d[Y_1A_1]}{dt} = \frac{2}{\gamma_T} k_{\text{on}}^{Y_1A_1} [Y_1][A_1] - k_{\text{off}}^{Y_1A_1} [Y_1A_1] \quad (17e)$$

$$\frac{d[Y_1A_1Y_1]}{dt} = \frac{\chi_1}{A_{\text{syn}} d_{\text{syn}} N_A} k_{\text{on}}^{Y_1A_1Y_1} [Y_1A_1][Y_1] - 2k_{\text{off}}^{Y_1A_1Y_1} [Y_1A_1Y_1] \quad (17f)$$

where Y , Y_1 and Y_2 represent PD-1, PD-L1, and PD-L2, respectively, and A and A_1 represent the antibodies to PD-1 and PD-L1, respectively. k_{on} and k_{off} are the binding constants, γ_T is volume fraction of interstitial space in tumor, χ is the intrinsic antibody cross-arm binding efficiency, A_{syn} is the surface area of the synapse, d_{syn} is the thickness of the confinement space between the two cells, and N_A is Avogadro's number. In this model, the effect of diffusion of the checkpoint molecules in and out of the synapse has been incorporated by overestimation of the size of the synapse.^{28,49} In addition, target-mediated drug disposition is neglected as it is thought that the antibodies of interest are in general in excess. For specific antibodies that are dosed in low concentrations, it might be necessary to implement the local degradation through target-mediated drug disposition.

PK module

The PK module aims to capture the population-averaged plasma concentrations of therapeutics, which are predicted

in published model-based population PK analyses, and predict their concentrations in the tumor.²⁸ This module is called directly by the corresponding PD module and does not need to be called by the user; at the time of this writing, the immune-checkpoint module is the only PD module implemented. The permeabilities between the central and the other compartments are estimated based on molecular weights of the therapeutics. The other PK parameters, including clearance rate and volume fractions of interstitial space available to the therapeutics, were determined for nivolumab using optimization using pattern search in the Global Optimization Toolbox in MATLAB to fit the plasma concentration^{28,50}; the PK parameters for other drugs will be added in future releases of QSP-IO.

The equations governing the PK of antibodies used in this tutorial are described as follows,

$$V_C \frac{d[A]_C}{dt} = \sum_{i=P,T,LN} Q_i \left(\frac{[A]_i}{\gamma_i} - \frac{[A]_C}{\gamma_C} \right) + Q_{LD} \frac{[A]_{LN}}{\gamma_{LN}} - k_{cl} [A]_C V_C \quad (18a)$$

$$V_P \frac{d[A]_P}{dt} = Q_P \left(\frac{[A]_C}{\gamma_C} - \frac{[A]_P}{\gamma_P} \right) \quad (18b)$$

$$\frac{d}{dt} (V_T [A]_T) = Q_T \left(\frac{[A]_C}{\gamma_C} - \frac{[A]_T}{\gamma_T} \right) - Q_{LD} \frac{[A]_T}{\gamma_T} \quad (18c)$$

$$V_{LN} \frac{d[A]_{LN}}{dt} = Q_{LN} \left(\frac{[A]_C}{\gamma_C} - \frac{[A]_{LN}}{\gamma_{LN}} \right) + Q_{LD} \frac{[A]_T}{\gamma_T} - Q_{LD} \frac{[A]_{LN}}{\gamma_{LN}} \quad (18d)$$

where Q_{LD} refers to the lymph flow rate from the tumor to the blood through lymph nodes^{38,51} k_{cl} is the clearance rate from central compartment; and γ_C , γ_P , γ_T , and γ_{LN} are the volume fractions of interstitial space available to the antibody in each compartment, respectively. The volumetric flow rates between central and other compartments in volume per time, Q_P , Q_T , and Q_{LN} , are calculated to be the product of the estimated permeability of the antibody and the total surface area of capillary walls.

EXAMPLE APPLICATIONS

In this section, we outline the procedure of developing a QSP model through two examples; the scripts for generating the examples can be found in the *scripts* directory included with this package. In both examples, we consider immune checkpoint therapy against PD-1 using the nivolumab antibody. The parameter values used in these examples were taken from the study by Jafarnejad *et al.*²⁸ with minor modifications.

SimBiology models are created using MATLAB scripts, which call various functions from QSP-IO. In general, scripts should perform the five following steps:

1. Load the parameters into the MATLAB workspace from the JSON file
2. Initialize the SimBiology model object
3. Call the individual modules to customize the model
4. Create the SimBiology dose object
5. Generate the initial conditions

In step 1, the parameters are loaded into the workspace by calling the `load_parameters` function that takes the file name as input. Next, in step 2, the SimBiology object is created by calling the `simbio_init` function. This function requires the model name, an array of time points at which to evaluate the simulation and the parameter structure that was created in step 1. Step 3 is where the structure of the model is defined by calling various modules; a summary of the modules currently included in QSP-IO and their dependencies is summarized in **Table 1**. In step 4, the SimBiology dose object is created; this object dictates which drugs are delivered, the time at which they are administered, and the dose of each drug. The dose object is created using the `schedule_dosing` function, which takes the names of drugs as input using a cell array of strings; at the time of this writing, nivolumab, durvalumab, and ipilimumab are currently supported; however, support for other common immunotherapy drugs will be added in the future. Optionally, the user may specify the patient weight, dose, and dose schedule through name–value pairs; the default information is hard-coded into that function as a lookup table and new drugs can be added by users by following the same format. Listing 2 shows example calls to the `schedule_dosing` function. Finally, the model is completed in step 5 by calling the `initial_conditions` function, which takes the model object as input and calculates the initial values for all the species in the model. Once the model object is created, it can be manipulated with any of the SimBiology functions. For example, the simulation can be run by calling the `sbiosimulate` function, which takes the model and dose objects as inputs. The results can be visualized using MATLAB's `plot` function or QSP-IO's `simbio_plot` function.

Listing 2: Examples of calling the schedule dose function

```
ds = schedule_dosing ({'nivolumab'}, 'patient-  
Weight', 90); % specify weight in kg  
ds = schedule_dosing ({'nivolumab', 'ipilim-  
umab'}); % specify two drugs  
% change dosing from default (3 mg/kg every two  
weeks ) to 1 mg/kg every week for 10 weeks  
sched = [0 ,7 ,10]; % format [ start_time , in-  
terval , number_of_repeats]  
ds = schedule_dosing ({'nivolumab'},  
'nivolumab_dose', 1, 'nivolumab_schedule',  
sched);
```

Example 1

In this first example, we simulate the response of a non-small cell lung cancer tumor to anti-PD-1 treatment. For this, we use the model in the study by Jafarnejad *et al.*²⁸ Their model considers cancer cells, T cells, Tregs, neo-antigens, self-antigens, antigen presentation, and the immune checkpoints (PD-1, PD-L1 and PD-L2). The script to create the model in this example is included with QSP-IO in the *example1.m* script file and is included in Listing 3 for

convenience. In step 1, the parameters for this model are loaded; the parameter values were taken from the study by Jafarnejad *et al.*²⁸ with minor modifications to account for small differences in the model structure. Steps 2, 4, and 5 follow exactly from the outline in Example Applications. For this example, in step 3, the cancer, T cell, Treg, APC, and antigen and immune checkpoint modules are called. The antigen module is called twice, once to create the neo-antigens and once to create a competing self-peptide. All of the modules take the SimBiology model object and a structure containing all of the model parameters as inputs. The cancer module requires an additional input that specifies a unique species name; this is required to allow for multiple subclones of cancer cells to be defined. The T cell module also requires two additional inputs: one that specifies a unique identifier for that specific T cell clone and one that specifies the name of the cancer cell subclones that it can recognize. The antigen module requires two additional inputs: a unique identifier and an antigen object that is created using the `create_antigen` function; the identifier is required to match that of a T cell clone. To define an antigen as a self-peptide, the identifier should be set to 0. The `create_antigen` function requires cancer subclone names that contain the antigen, the intracellular antigen concentration in the cancer cell and optionally, the user may specify an identifier that uses a lookup table to assign the binding rate constants for the antigen to MHC molecules. The immune checkpoint module requires two additional inputs: one that specifies the name of the T cell clone and one that specifies the name of the cancer subclone. Optionally, the user may specify the names of antibodies to PD-1 or PD-L1 (see line 30 of Listing 3); if the user does not specify any antibodies, no antibodies are simulated.

Listing 3: Example 1 script

```
% Model Settings  
model_name = 'Immune Oncology Model';  
start_time = 0.0; % solution start time [days]  
  
% Load Model Parameters (Step 1)  
parameter_filename = 'parameters/example1_pa-  
rameters.json';  
params = load_parameters (parameter_filename);  
Model Initialization (Step 2)  
time = start_time : time_step : end_time;  
model = simbio_init (model_name, time, params);  
  
% Add Modules (Step 3)  
  
% Cancer Module  
model = cancer_module (model , 'C1', params);  
  
% T Cell Module  
model = Tcell_module (model, '1', params, {'C1'});  
  
% T Reg Module  
model = Treg_module (model, params);
```

```

% APC Module
model = APC_module (model, params);

% Antigen Module
self_antigen = create_antigen ({'C1'}, 1e -8,
'antigenID',0);
neo_antigen = create_antigen ({'C1'}, 1e -8,
'antigenID',1);
model = antigen_module (model , '0', params,
self_antigen);
model = antigen_module (model, '1', params,
neo_antigen);

% PD1 Immune Checkpoint Module
model = PD1_module (model, params, 'T1', 'C1',
'drugName', 'nivolumab');

% Dose Schedule (Step 4)
dose_schedule = schedule_dosing ({'nivolumab'});

% Generate Initial Conditions (Step 5)
model = initial_conditions (model);

```

Figure 3 shows the results of anti-PD-1 treatment and no treatment for this example model. Both simulations use the same parameterization, the only difference being that no dose object is specified for the no-treatment simulation. The

parameters for the example were hand tuned to give a parameterization that simulates a virtual patient that responds to treatment. The tumor in the no-treatment case grows exponentially, whereas in the treatment case, the tumor decreases in size. The number of cancer cells in the treatment case decreases faster than the tumor volume because of the presence of dead cancer cells and T cells in the tumor. The amount of antigen present in the tumor compartment is much larger in the no-treatment case because the rate of cancer cell death is higher. The density of T cells and Tregs in the tumor reach maximum and decrease because the naïve T cells/Tregs in the blood are limited by their thymic output.

To show the variability in the dynamics of the model, we simulated 100 parameterizations of the model using a Latin hypercube sampling of 10 parameters (**Figure 4**). The range for each parameter was chosen to be physiologically realistic; see **Table 2** for more details. **Figure 4** also shows the simulation results in terms of the percent change in tumor diameter both as a function time for 400 days (**Figure 4b**) and after 60 days of treatment (**Figure 4d**) because these are frequently reported in clinical studies and are used for assessing patient response to therapy. The Response Evaluation Criteria In Solid Tumors (RECIST), often used as a metric for evaluating tumor response to therapy, is shown as a function of time (**Figure 4c**); this demonstrates the sensitivity of this metric on the time of measurement. In this study, RECIST criteria are calculated assuming a single lesion for which the diameter is assumed to be the diameter of sphere with the

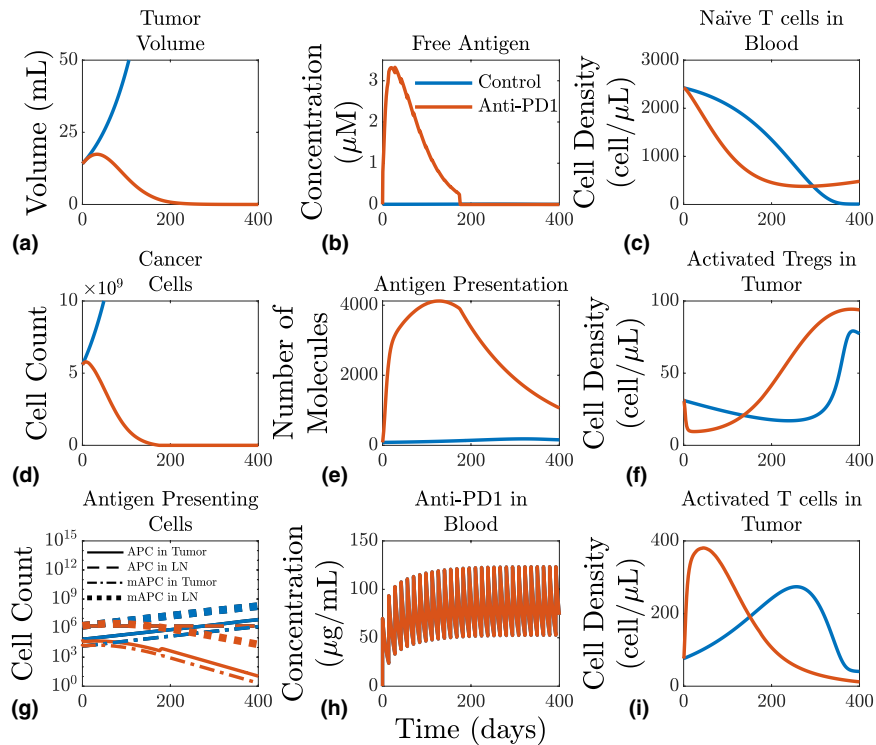


Figure 3 Simulation results as a function of time for control (blue) and anti-PD-1 treatment (red). (a) Tumor volume. (b) Concentration of free antigen in the tumor. (c) Naïve T cell density in the blood. (d) Number of cancer cells. (e) Number of antigen-MHC complex molecules per APC binding site. (f) Activated Treg density in the blood. (g) Number of APCs. (h) Concentration of nivolumab in the blood. (i) Activated T cell density in the tumor. APC, antigen presenting cell; LN, lymph node compartment; mAPC, mature antigen presenting cell; PD-1, programmed cell death protein 1; Tregs, regulatory T cells.

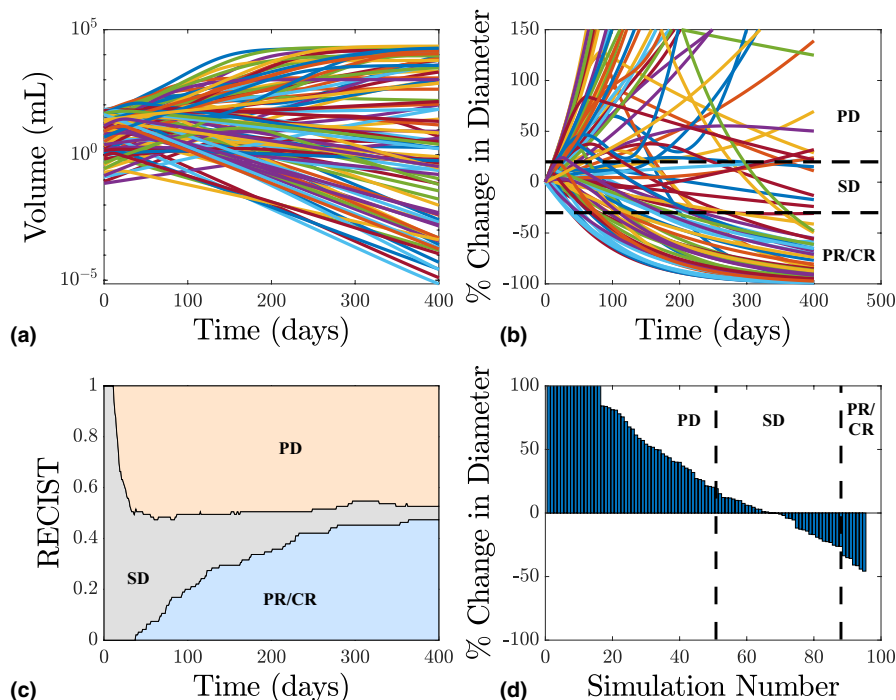


Figure 4 (a) Tumor volume as a function of time for a Latin hypercube sampling (LHS) ($n = 100$) of a subset of the parameter space; 5 of the 100 parameterizations did not reach the initial tumor diameter. Ten parameters were varied over a physiological range; see **Table 2**. (b) Percent change in tumor diameter as a function of time for the LHS. Dashed lines indicate the threshold for the Response Evaluation Criteria In Solid Tumors (RECIST); regions are labeled with PR/CR for partial/complete response, SD for stable disease, and PD for progressive disease. (c) RECIST values as a function of time for the LHS. (d) Waterfall plot showing the percent change in diameter at 60 days following the start of treatment. Each bar represents a simulation, with height representing the percent change in tumor diameter.

Table 2 Parameter ranges used to generate the Latin hypercube sampling of parameter space for Figure 4

Description	Parameter	Variable name	Range
Cancer cell growth rate	k_{growth}	k_C1_growth	0.001–0.05 day ⁻¹
Cancer cell capacity	C_{max}	C_max	10 ¹¹ –10 ¹³ cells
Initial tumor diameter	$D_{\text{T}}(0)$	initial_tumor_diameter	0.5–5.0 cm
Number of T cell clones	n_{clones}	n_T1_clones	1–1000
Rate of thymic output	σ	Q_nT1_thym	10 ⁸ –10 ¹⁰
Cancer cell death rate from T cells	k_{Tcell}	k_C_T1	0.5–50 day ⁻¹
T cell cell death rate	$k_{\text{death}}^{\text{T}}$	k_T1_death	0.01–10 day ⁻¹
T cell transport rate out of the lymph nodes	$q_{\text{LN}}^{\text{out}}$	q_T1_LN_out	0.1–10 day ⁻¹
Cell clearance rate	k_{clear}	k_cell_clear	0.001–0.04 day ⁻¹
Number of PD1-PDL1 complex molecules for half-maximal inhibition of T cell cytotoxicity	$PD1_{50}$	PD1_50	1–50 molecules

same volume as the tumor; this approach was taken in previous work.^{26–28} Note that because we sampled the parameter space uniformly, the distribution of virtual patient responses shown in **Figure 4** does not reflect clinical outcomes. To simulate a virtual clinical trial, the distribution from which the parameters must be sampled needs to be determined. Potential approaches for determining parameter distributions for simulating clinical trials are implemented in refs. 52–54

Example 2

In this second example, we consider a patient with two different cancer cell clones: one with a larger growth rate than the other. We also consider two different cytotoxic T cell

clones: the first clone will only recognize one of the cancer clones, and the second clone recognizes both cancer cell clones. Finally, we simulate 1 year of therapy and follow the tumor progression after the end of treatment. To construct this model, we need to call the cancer module twice, modifying the growth rate for the second call, and the T cell module twice, modifying the rate at which the T cells kill the cancer cells for the second call. We also need to call the immune checkpoint module and create the dose object. For simplicity, this example will not consider antigen presentation or the presence of Tregs.

Figure 5 shows the simulation results for example 2. In the no-treatment case, the tumor increases rapidly until it

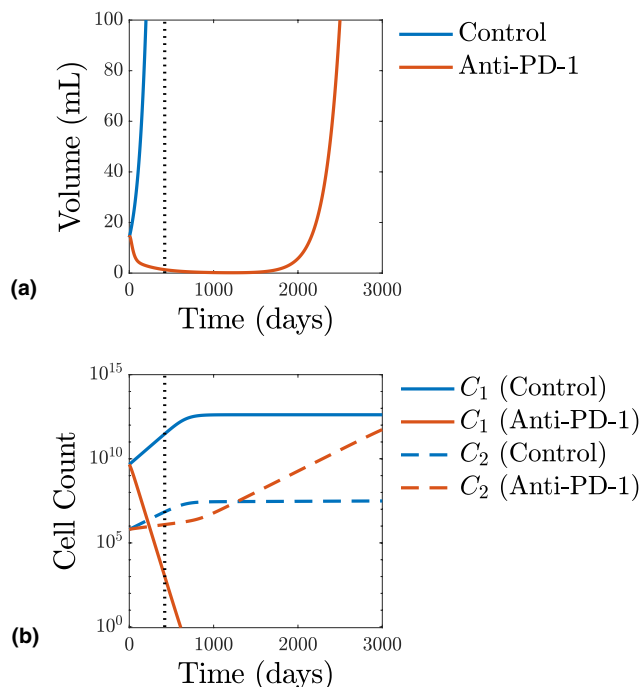


Figure 5 Simulation of a patient with two different cancer cell clones, C_1 and C_2 , where C_2 has a slower growth rate and lower rate of death from T cells. The simulation is run over approximately 8 years (3,000 days), with treatment given for 1 year. (a) Tumor volume as a function of time. (b) Number of cancer cells as a function of time. The vertical dotted line indicates the end of the treatment.

asymptotically approaches the cancer cell capacity dictated by C_{\max} . In the case of anti-PD-1 treatment, the tumor increases in size at the beginning of treatment, followed by a rapid decrease in size. Shortly after the end of the treatment, the C_1 cancer cells are eliminated, leaving only a small (on the order of 10^5) number of C_2 cells, which go on to grow exponentially.

CONCLUSIONS

Following our experience in developing and publishing QSP models for immunotherapy applications, we identified sources that limit the implementation of QSP models for decision-making in drug development and attempted to address this problem through the introduction of a new open-source platform we called QSP-IO. In this tutorial, we introduced the rationale behind the structure of the modeling framework focused on explaining the individual modules and finished by showing two examples to demonstrate the capabilities of QSP-IO. The framework was designed to allow easy expansion of the model and facilitate adoption and modification of the modules by the industry and academic users. The assumptions behind mathematical representation of each biological process were explained in detail for each module.

Development of this open-source, modular, and expandable toolbox that is being actively verified and validated through regular use and rigorous peer review could facilitate the resolution of a number of limitations facing wider

spread use of QSP models. The reusability of the verified modules reduces the time from conception of the problem to the production of practical results for decision making. The modular platform allows the user to select and refine the minimal model required to address the questions at hand, which reduces the uncertainty from too many degrees of freedom and makes the model fit for purpose. The modular platform also allows the developers and users to expand the features of the model over time to make the toolbox suitable for a variety of targets relevant in the IO area.

Despite all the improvements provided by the QSP-IO platform, there are a number of areas for further improvement in the toolbox. For example, the current QSP-IO models can investigate the efficacy of the immune checkpoint-blocking therapeutics, but toxicity modules are necessary to enable the optimization of the dosing schedule as implemented in refs. 55–57. Furthermore, to facilitate the translation of pre-clinical animal experimental findings to humans, a parallel parameterization of the model for mice is required to enable the users to exploit the relatively rich data sets from mice for prediction of the response in humans.

In addition, current modules could be improved to include more biological mechanisms. For instance, the immune checkpoint module could be augmented by allowing for checkpoint expression to be dependent on the tumor immune microenvironment, for example, PD-L1 expression on cancer cells has been shown to be induced by the presence of interferon gamma.^{58–61} In addition, other important checkpoint pathways could be included such as CTLA-4 and tumor necrosis factor receptor superfamily member 4 (TNFRSF4, also known as OX-40). Models of CTLA-4 pathways have been implemented in refs. 62 and 63. A pathway model for OX-40 can be developed using similar methodology based on our current understanding of the biology.^{64–66}

Thus far, our efforts have focused on immune-checkpoint therapy, and therefore we have developed detailed mechanistic models of T cells; however, currently, QSP-IO does not explicitly have modules for innate immune cells such as NK cells, macrophages, or myeloid-derived suppressor cells. Models for NK cells^{55,67–69} and macrophages^{69,70} have been implemented in previous studies, and we plan to add modules for macrophages and NK cells based on these studies that will be available in future releases of QSP-IO.

In conclusion, QSP-IO serves as the first step toward a more comprehensive framework to run virtual clinical trials. A second follow-up tutorial is planned for release of an update for the toolbox to enable the user to utilize the model developed by QSP-IO to generate plausible patient populations and select a virtual patient population that captures the known variability in actual patient populations in the clinical trials.

Supporting Information. Supplementary information accompanies this paper on the *CPT: Pharmacometrics & Systems Pharmacology* website (www.psp-journal.com).

Funding. This work was supported by National Institutes of Health Grants U01CA212007 and R01CA138264.

Conflict of Interest. The authors declared no competing interests for this work.

- Farkona, S., Diamandis, E.P. & Blasutig, I.M. Cancer immunotherapy: the beginning of the end of cancer? *BMC Med.* **14**, 73 (2016).
- Marshall, H.T. & Djamgoz, M.B.A. Immuno-oncology: emerging targets and combination therapies. *Front Oncol.* **8**, 315 (2018).
- Darvin, P., Toor, S.M., Sasidharan Nair, V. & Elkord, E. Immune checkpoint inhibitors: recent progress and potential biomarkers. *Exp. Mol. Med.* **50**, 1–11 (2018).
- Popovic, A., Jaffee, E.M. & Zaidi, N. Emerging strategies for combination checkpoint modulators in cancer immunotherapy. *J. Clin. Invest.* **128**, 3209–3218 (2018).
- Wei, S.C., Duffy, C.R. & Allison, J.P. Fundamental mechanisms of immune checkpoint blockade therapy. *Cancer Discov.* **8**, 1069–1086 (2018).
- Marin-Acevedo, J.A., Dholaria, B., Soyano, A.E., Knutson, K.L., Chumsri, S. & Lou, Y. Next generation of immune checkpoint therapy in cancer: new developments and challenges. *J. Hematol. Oncol.* **11**, 39 (2018).
- Guerriero, J.L. Macrophages: the road less traveled, changing anticancer therapy. *Trends Mol. Med.* **24**, 472–489 (2018).
- van Willigen, W.W., Bloemendal, M., Gerritsen, W.R., Schreiberlt, G., de Vries, I.J.M. & Bol, K.F. Dendritic cell cancer therapy: vaccinating the right patient at the right time. *Front. Immunol.* **9**, 2265 (2018).
- Joshi, S. & Durden, D.L. Combinatorial approach to improve cancer immunotherapy: rational drug design strategy to simultaneously hit multiple targets to kill tumor cells and to activate the immune system. *J. Oncol.* **2019**, 5245034 (2019).
- Fukumura, D., Kloepper, J., Amoozgar, Z., Duda, D.G. & Jain, R.K. Enhancing cancer immunotherapy using antiangiogenics: opportunities and challenges. *Nat. Rev. Clin. Oncol.* **15**, 325–340 (2018).
- Wang, M., Liu, Y., Cheng, Y., Wei, Y. & Wei, X. Immune checkpoint blockade and its combination therapy with small-molecule inhibitors for cancer treatment. *Biochim. Biophys. Acta Rev. Cancer* **1871**, 199–224 (2019).
- Tang, J., Shalabi, A. & Hubbard-Lucey, V.M. Comprehensive analysis of the clinical immuno-oncology landscape. *Ann. Oncol.* **29**, 84–91 (2018).
- Tang, J., Yu, J.X., Hubbard-Lucey, V.M., Neftelinov, S.T., Hodge, J.P. & Lin, Y. Trial watch: the clinical trial landscape for PD1/PDL1 immune checkpoint inhibitors. *Nat. Rev. Drug Discov.* **17**, 854–855 (2018).
- Yi, M. et al. Biomarkers for predicting efficacy of PD-1/PD-L1 inhibitors. *Mol. Cancer* **17**, 129 (2018).
- Peskov, K., Azarov, I., Chu, L., Voronova, V., Kosinsky, Y. & Helmlinger, G. Quantitative mechanistic modeling in support of pharmacological therapeutics development in immuno-oncology. *Front. Immunol.* **10**, 924 (2019).
- Klinke, D.J. Enhancing the discovery and development of immunotherapies for cancer using quantitative and systems pharmacology: interleukin-12 as a case study. *J. Immunother. Cancer* **3**, 27 (2015).
- Cheng, Y. et al. QSP toolbox: computational implementation of integrated workflow components for deploying multi-scale mechanistic models. *AAPS J.* **19**, 1002–1016 (2017).
- Nijssen, M.J.M.A. et al. Preclinical QSP modeling in the pharmaceutical industry: an IQ consortium survey examining the current landscape. *CPT Pharmacometrics Syst. Pharmacol.* **7**, 135–146 (2018).
- Bai, J.P.F., Earp, J.C. & Pillai, V.C. Translational quantitative systems pharmacology in drug development: from current landscape to good practices. *AAPS J.* **21**, 72 (2019).
- Marshall, S. et al. Model-informed drug discovery and development: current industry good practice and regulatory expectations and future perspectives. *CPT Pharmacometrics Syst. Pharmacol.* **8**, 87–96 (2019).
- Mentre, F. et al. Pharmacometrics and systems pharmacology 2030. *Clin. Pharmacol. Therapeut.* **107**, 76–78 (2020).
- Visser, S.A., de Alwis, D.P., Kerbusch, T., Stone, J.A. & Allerheiligen, S.R. Implementation of quantitative and systems pharmacology in large pharma. *CPT Pharmacometrics Syst. Pharmacol.* **3**, e142 (2014).
- Rockne, R.C. et al. A patient-specific computational model of hypoxia-modulated radiation resistance in glioblastoma using 18F-FMISO-PET. *J. R. Soc. Interface* **12**, 20141174 (2015).
- Helmlinger, G. et al. Quantitative systems pharmacology: an exemplar model-building workflow with applications in cardiovascular, metabolic, and oncology drug development. *CPT Pharmacometrics Syst. Pharmacol.* **8**, 380–395 (2019).
- Jarrett, A.M. et al. Experimentally-driven mathematical modeling to improve combination targeted and cytotoxic therapy for HER2+ breast cancer. *Sci. Rep.* **9**, 12830 (2019).
- Wang, H. et al. In silico simulation of a clinical trial with anti-CTLA-4 and anti-PD-L1 immunotherapies in metastatic breast cancer using a systems pharmacology model. *R. Soc. Open Sci.* **6**, 190366 (2019).
- Milberg, O. et al. A QSP model for predicting clinical responses to monotherapy, combination and sequential therapy following CTLA-4, PD-1, and PD-L1 checkpoint blockade. *Sci. Rep.* **9**, 11286 (2019).
- Jafarnejad, M. et al. A computational model of neoadjuvant PD-1 inhibition in non-small cell lung cancer. *AAPS J.* **21**, 79 (2019).
- Wang, H. et al. Conducting a virtual clinical trial in HER2-negative breast cancer using a quantitative systems pharmacology model with an epigenetic modulator and immune checkpoint inhibitors. *Front. Bioeng. Biotechnol.* **8**, 141 (2020).
- Ma, H. et al. A quantitative systems pharmacology model of T cell engager applied to solid tumor. *AAPS J.* **22**, 85 (2020).
- Sorger, P.K. et al. Quantitative and Systems Pharmacology in the Post-Genomic Era: New Approaches to Discovering Drugs and Understanding Therapeutic Mechanisms. QSP Workshop Group White Paper Vol. **48** (National Institutes of Health, Bethesda, MD, 2011).
- Helmlinger, G. et al. Drug-disease modeling in the pharmaceutical industry - where mechanistic systems pharmacology and statistical pharmacometrics meet. *Eur. J. Pharm. Sci.* **109S**, S39–S46 (2017).
- Sarapata, E.A. & de Pillis, L.G. A comparison and catalog of intrinsic tumor growth models. *Bull. Math. Biol.* **76**, 2010–2024 (2014).
- de Pillis, L., Gallegos, A. & Radunskaya, A. A model of dendritic cell therapy for melanoma. *Front. Oncol.* **3**, 56 (2013).
- Chiou, V.L. & Burotto, M. Pseudoprogression and immune-related response in solid tumors. *J. Clin. Oncol.* **33**, 3541–3543 (2015).
- Russo, E. et al. Intralymphatic CCL21 promotes tissue egress of dendritic cells through afferent lymphatic vessels. *Cell Rep.* **14**, 1723–1734 (2016).
- Weber, M. et al. Interstitial dendritic cell guidance by haptotactic chemokine gradients. *Science* **339**, 328–332 (2013).
- Jafarnejad, M., Zawieja, D.C., Brook, B.S., Nibbs, R.J.B. & Moore, J.E. A novel computational model predicts key regulators of chemokine gradient formation in lymph nodes and site-specific roles for CCL19 and ACKR4. *J. Immunol.* **199**, 2291–2304 (2017).
- Chen, X., Hickling, T.P. & Vicini, P. A mechanistic, multiscale mathematical model of immunogenicity for therapeutic proteins: part 1-theoretical model. *CPT Pharmacometrics Syst. Pharmacol.* **3**, e133 (2014).
- Chen, X., Hickling, T.P. & Vicini, P. A mechanistic, multiscale mathematical model of immunogenicity for therapeutic proteins: part 2-model applications. *CPT Pharmacometrics Syst. Pharmacol.* **3**, e134 (2014).
- Agrawal, N.G. & Linderman, J.J. Mathematical modeling of helper T lymphocyte/antigen-presenting cell interactions: analysis of methods for modifying antigen processing and presentation. *J. Theor. Biol.* **182**, 487–504 (1996).
- den Braber, I. et al. Maintenance of peripheral naive T cells is sustained by thymus output in mice but not humans. *Immunity* **36**, 288–297 (2012).
- Bains, I., Antia, R., Callard, R. & Yates, A.J. Quantifying the development of the peripheral naive CD4+ T-cell pool in humans. *Blood* **113**, 5480–5487 (2009).
- Lever, M., Maini, P.K., van der Merwe, P.A. & Dushek, O. Phenotypic models of T cell activation. *Nat. Rev. Immunol.* **14**, 619–629 (2014).
- Marchingo, J.M. et al. T cell signaling. Antigen affinity, costimulation, and cytokine inputs sum linearly to amplify T cell expansion. *Science* **346**, 1123–1127 (2014).
- Zhu, H., Melder, R.J., Baxter, L.T. & Jain, R.K. Physiologically based kinetic model of effector cell biodistribution in mammals: implications for adoptive immunotherapy. *Cancer Res.* **56**, 3771–3781 (1996).
- Fouchet, D. & Regoes, R. A population dynamics analysis of the interaction between adaptive regulatory T cells and antigen presenting cells. *PLoS One* **3**, e2306 (2008).
- Churlaud, G. et al. Human and mouse CD8(+)/CD25(+)/FOXP3(+) regulatory T cells at steady state and during interleukin-2 therapy. *Front. Immunol.* **6**, 171 (2015).
- Cheng, X. et al. Structure and interactions of the human programmed cell death 1 receptor. *J. Biol. Chem.* **288**, 11771–11785 (2013).
- Bazzazi, H., Zhang, Y., Jafarnejad, M., Isenberg, J.S., Annex, B.H. & Popel, A.S. Computer simulation of TSP1 inhibition of VEGF-Akt-eNOS: An Angiogenesis Triple Threat. *Front. Physiol.* **9**, 644 (2018).
- Jafarnejad, M., Woodruff, M.C., Zawieja, D.C., Carroll, M.C. & Moore, J.E. Modeling lymph flow and fluid exchange with blood vessels in lymph nodes. *Lymphat. Res. Biol.* **13**, 234–247 (2015).
- Klinke, D.J. Integrating epidemiological data into a mechanistic model of type 2 diabetes: validating the prevalence of virtual patients. *Ann. Biomed. Eng.* **36**, 321–334 (2008).
- Schmidt, B.J., Casey, F.P., Paterson, T. & Chan, J.R. Alternate virtual populations elucidate the type I interferon signature predictive of the response to rituximab in rheumatoid arthritis. *BMC Bioinformatics* **14**, 221 (2013).
- Allen, R.J., Rieger, T.R. & Musante, C.J. Efficient Generation and Selection of Virtual Populations in Quantitative Systems Pharmacology Models. *CPT Pharmacometrics Syst. Pharmacol.* **5**, 140–146 (2016).
- Cappuccio, A., Elishmereni, M. & Agur, Z. Cancer immunotherapy by interleukin-21: potential treatment strategies evaluated in a mathematical model. *Cancer Res.* **66**, 7293–7300 (2006).
- Cappuccio, A., Elishmereni, M. & Agur, Z. Optimization of interleukin-21 immunotherapeutic strategies. *J. Theor. Biol.* **248**, 259–266 (2007).
- Castiglione, F. & Piccoli, B. Cancer immunotherapy, mathematical modeling and optimal control. *J. Theor. Biol.* **247**, 723–732 (2007).
- Chen, J. et al. Interferon- γ -induced PD-L1 surface expression on human oral squamous carcinoma via PKD2 signal pathway. *Immunobiology* **217**, 385–393 (2012).

59. Abiko, K. *et al.* IFN- γ from lymphocytes induces PD-L1 expression and promotes progression of ovarian cancer. *Br. J. Cancer* **112**, 1501–1509 (2015).
60. Garcia-Diaz, A. *et al.* Interferon receptor signaling pathways regulating PD-L1 and PD-L2 expression. *Cell Rep.* **19**, 1189–1201 (2017).
61. Mimura, K. *et al.* PD-L1 expression is mainly regulated by interferon gamma associated with JAK-STAT pathway in gastric cancer. *Cancer Sci.* **109**, 43–53 (2018).
62. Jansson, A. *et al.* A theoretical framework for quantitative analysis of the molecular basis of costimulation. *J. Immunol.* **175**, 1575–1585 (2005).
63. Jansson, A. & Davis, S.J. Quantitative analysis predicts the relative therapeutic efficacy of different forms of CTLA4lg. *Mol. Immunol.* **49**, 527–536 (2011).
64. Gramaglia, I., Jember, A., Pippig, S.D., Weinberg, A.D., Killeen, N. & Croft, M. The OX40 costimulatory receptor determines the development of CD4 memory by regulating primary clonal expansion. *J. Immunol.* **165**, 3043–3050 (2000).
65. Maxwell, J.R., Weinberg, A., Prell, R.A. & Vella, A.T. Danger and OX40 receptor signaling synergize to enhance memory T cell survival by inhibiting peripheral deletion. *J. Immunol.* **164**, 107–112 (2000).
66. Zhang, P. *et al.* Ligand-blocking and membrane-proximal domain targeting anti-OX40 antibodies mediate potent T cell-stimulatory and anti-tumor activity. *Cell Rep.* **27**, 3117–3123 (2019).
67. Merrill, S.J. A model of the role of natural killer cells in immune surveillance—I. *J. Math Biol.* **12**, 363–373 (1981).
68. de Pillis, L.G., Radunskaya, A.E. & Wiseman, C.L. A validated mathematical model of cell-mediated immune response to tumor growth. *Cancer Res.* **65**, 7950–7958 (2005).
69. Lai, X., Stiff, A., Duggan, M., Wesolowski, R., Carson, W.E. & Friedman, A. Modeling combination therapy for breast cancer with BET and immune checkpoint inhibitors. *Proc. Natl. Acad. Sci. USA* **115**, 5534–5539 (2018).
70. Palsson, S. *et al.* The development of a fully-integrated immune response model (FIRM) simulator of the immune response through integration of multiple subset models. *BMC Syst. Biol.* **7**, 95 (2013).

© 2020 The Authors. *CPT: Pharmacometrics & Systems Pharmacology* published by Wiley Periodicals LLC on behalf of the American Society for Clinical Pharmacology and Therapeutics. This is an open access article under the terms of the Creative Commons Attribution-NonCommercial License, which permits use, distribution and reproduction in any medium, provided the original work is properly cited and is not used for commercial purposes.